In situ characterization of β″ precipitation in an Al–Mg–Si alloy by anisotropic small-angle neutron scattering on a single crystal

Cynthia Sin Ting Chang,[a] Frédéric De Geuser[b,c] and John Banhart[d,a]*

[a]Materials Science and Technology, Technische Universität Berlin, Hardenbergstrasse 36, Berlin, 10623, Germany, [b]CNRS, SIMAP, Grenoble, 38000, France, [c]Université Grenoble Alpes, SIMAP, Grenoble, 38000, France, and [d]Applied Materials, Helmholtz-Zentrum Berlin, Hahn-Meitner Platz, Berlin, 14109, Germany. Correspondence e-mail: john.banhart@tu-berlin.de

A single crystal of an Al–Mg–Si alloy (Mg: 0.43 wt%, Si: 0.47 wt%) was aged at 453 K while small-angle neutron scattering experiments were carried out *in situ*. The scattering data recorded on a two-dimensional detector show the symmetry typical for needle-shaped β″ precipitates oriented in the three [100] directions of the aluminium lattice and allow the calculation of the length, diameter and number density of the precipitates assuming cylindrical scattering objects of equal size and composition. The repetition time of the experiments was ~12 min. The values obtained for the three quantities agree well with values measured by transmission electron microscopy (TEM) on a similar alloy. The impact of one week of natural ageing before artificial ageing on the evolution of the size and number density of precipitates is found to be pronounced, as expected from published TEM data.

1. Introduction

Age hardening is used to increase the mechanical strength of aluminium alloys. After solutionizing and quenching, an alloy is exposed to 'artificial ageing' (AA), during which the supersaturated solid solution decomposes in various stages, eventually forming a dense distribution of metastable hardening precipitates. In the common alloy group Al–Mg–Si, needle-shaped β″ precipitates are formed at 453 K within a few hours to one day. The details of the precipitation sequence depend very much on the exact alloy composition and thermal history. If an alloy is subject to 'natural ageing' (NA) at 'room temperature' (*i.e.* around 293 K), the subsequent ageing process is notably modified (Gayler & Preston, 1929; Brenner & Kostron, 1939; Pashley *et al.*, 1966).

The structure and composition of such precipitates have been studied by transmission electron microscopy (TEM) and atom probe tomography. Nowadays the precipitation sequence is largely understood, but there is still some dispute about the influence of NA treatments prior to AA. The β″ precipitates formed during AA (with and without preceding NA) have been characterized with respect to their structure, composition, size and number density (see *Discussion* for details and references). While the various literature sources agree on the general trends, the absolute values of the measured precipitate dimensions and number densities scatter very much. Data are usually collected only for a small number of samples, and every TEM measurement corresponds to a different specimen and to a very small probed volume. This leads to uncertainties and a lack of confidence in the data.

For a quantitative statistical analysis of precipitation, small-angle scattering is an obvious alternative, which is why it has found ample application since the 1950s (Guinier & Fournet, 1955). Small-angle scattering probes a volume vastly larger than that probed by local techniques such as TEM, allowing for statistically more meaningful size measurements. For Al–Mg–Si alloys, however, the very low scattering contrast between the elements makes the use of X-rays difficult. Although application of small-angle X-ray scattering (SAXS) to the precipitation kinetics in commercial Al–Mg–Si-based alloys has been reported (Tsao *et al.*, 2006), Al–Mg–Si alloys are generally considered poor candidates for SAXS experiments (Bardel *et al.*, 2014). Anomalous SAXS, successfully applied to some aluminium alloys (Lyon *et al.*, 1983; De Geuser & Deschamps, 2012), could be an option to improve the very weak contrast, but the very low *K*-edge energies of Al, Mg and Si makes this a difficult task. Therefore, small-angle neutron scattering (SANS) appears to be more promising. The scattering contrast between the three elements is not very large, but thick samples can give enough scattering signal to detect precipitates. Polycrystalline samples that have been aged for different times and temperatures have been investigated *ex situ* by SANS by different groups (Abis *et al.*, 1985; Donnadieu *et al.*, 1998; Albertini *et al.*, 2000; Schiffmann *et al.*, 2004; Ohnuma & Suzuki, 2006). The measured scattering data have been fitted by models based on a distribution of spheres (Abis *et al.*, 1985; Schiffmann *et al.*, 2004) or cylinders randomly oriented in space (Abis *et al.*, 1985; Donnadieu *et al.*, 1998) to obtain distributions and size and shape parameters of the precipitates.

The random orientation and the large aspect ratio of the needle-shaped β'' precipitates makes it difficult to derive independent information on the length L and thickness D distributions of such objects. One of the reasons is that it is close to impossible to use an experimental setup that covers a scattering vector range wide enough to resolve the long dimension and the short dimension at the same time. Therefore, Abis *et al.* (1987) attempted to use oriented single crystals instead of polycrystals. If one of the [100] directions is oriented in parallel to the neutron beam, two variants of the needles are perpendicular to the beam and to each other and the third is parallel to the beam. Although they did not succeed in presenting an analysis of L and D, the approach was shown to be promising because, by using the intrinsic two-dimensional information, dimensions larger than what is usually available with a given minimum scattering vector can be measured (Fratzl *et al.*, 1993; De Geuser *et al.*, 2012).

The drawback of characterizing different samples aged for various times *ex situ* is the usually low number of samples probed and possible fluctuations between individual samples. Therefore, an experiment was designed in which an Al–Mg–Si alloy single crystal is artificially aged while continuously recording *in situ* the neutron scattering pattern to obtain the distributions of length and diameter of the precipitates with a good time resolution. The experiment was carried out twice: once while ageing the sample directly after quenching and once while ageing after the sample had been naturally aged after quenching.

A first analysis of the experimental data was based on intensity profiles taken along two special angular sectors of the two-dimensional SANS images. The analysis showed the anisotropy of scattering and allowed for a qualitative discussion of the effect of NA before AA (Chang *et al.*, 2012). However, no precipitate sizes and densities were obtained. In this paper, we describe the full experiment and data interpretation and discuss the effects of artificial and natural ageing on an Al–Mg–Si alloy.

2. Experimental

2.1. Sample preparation

A single crystal was prepared by remelting an alloy containing nominally 0.6 wt% Mg and 0.8 wt% Si. This alloy has been studied previously (Banhart *et al.*, 2010, 2011). The alloy was melted in a crucible, after which a single crystal was extracted by directional solidification. The rod obtained was 16 mm thick and 120 mm long. The crystallographic orientation was measured by Laue diffraction. For this, the rod was mounted on a goniometer and rotated until a [100] direction had been identified. Then, a 4.55 mm-thick slice was cut out of the bar so that the [100] direction of the crystal lattice was oriented perpendicular to the surface. The resulting slice was 48 mm long owing to the high angle between the crystallographic and geometrical axes of the rod. Before the SANS experiment, the sample was homogenized at 773 K for 12 h.

The chemical composition at the centre of the slice was determined by inductively coupled plasma atomic emission spectroscopy at Hydro Aluminium (Bonn, Germany) after the SANS measurements had been completed. The actual composition found was 0.43 wt% Mg and 0.47 wt% Si, indicating large deviations from the original composition of the remelted alloy. Composition measurements at both ends of the single-crystal rod from which the sample for SANS had been cut confirmed a concentration gradient along its axis. As the sample for SANS was extracted from a plane that formed an angle of just 20° with the axis of the rod, the concentration gradients were geometrically magnified. We estimate that the variation of Mg and Si composition over the area probed by SANS (10 mm diameter) is at the most 0.05% or below (in absolute percentages), which has to be related to the concentrations of Mg (0.43%) and Si (0.47%). The neutron beam therefore probed an area with slightly spread out concentrations, and the measured signal represents a convolution of ageing kinetics corresponding to a range of compositions centred around the average concentration. It is expected that this does broaden the distribution of precipitation lengths and widths but does not affect the present results since only average precipitate parameters are determined.

2.2. SANS measurements

Beamline D22 at the Institute Laue–Langevin (ILL), Grenoble, France, was used for small-angle neutron scattering. The measurement position was equipped with a hot plate for *in situ* ageing at 453 K. To cover a wide scattering vector magnitude (q) range, two sample-to-detector distances were chosen, 1.4 and 5.6 m. The neutron wavelength selected was $\lambda = 0.5$ nm with $\Delta\lambda/\lambda = 0.1$, and the detector was 102.4×98 cm in size. The q range covered was therefore about 0.15–4.1 nm^{-1}. Background subtractions, data reduction and absolute normalization were performed using the software $GRAS_{ans}P$ (Dewhurst, 2008), which is based on MATLAB (The MathWorks Inc., Natick, MA, USA). The subsequent two-dimensional model fitting was performed through in-house written MATLAB scripts. As the (111) Bragg edge in face-centred cubic aluminium lies at $\lambda = [2(3^{1/2})/3] \times 0.405$ nm = 0.468 nm, only marginal anisotropic scattering is expected.

Two full measurements of precipitation kinetics were carried out. The sample was first solutionized at 813 K for 60 min and then quenched in ice water and aged for one week at room temperature, *i.e.* at approximately 293 K (before the measurement campaign). After this, the first *in situ* ageing experiment with simultaneous SANS measurement was carried out. The time needed for the sample to reach 453 K was estimated to be less than 1 min. For the first 30 min of the experiment, images were acquired every minute at the shortest detector distance (1.4 m). Then, 5 min acquisitions were obtained continuously, alternating between 1.4 m and 5.6 m for the remaining experiment (about 18 h). Counting the time needed to change the detector distance, this leads to a

total time for acquiring a complete composite data set of ~12 min. After this experiment, the sample was re-solutionized and quenched and directly mounted on the setup for a second ageing experiment. The time at room temperature between quench and the onset of ageing was below 5 min. The SANS acquisitions were performed in exactly the same way as in the first experiment. The two experiments will be labelled 'NA + AA' and 'AA' in the following.

2.3. SANS data analysis

The SANS intensity I_{cyl} of a cylinder of diameter D and length L can be written as (Guinier & Fournet, 1955)

$$I_{cyl} = \Delta\rho^2 V^2 \left| \sin\left(\frac{L}{2}q_L\right) \bigg/ \left(\frac{L}{2}q_L\right) \right|^2 \left| 2J_1\left(\frac{D}{2}q_D\right) \bigg/ \left(\frac{D}{2}q_D\right) \right|^2,$$

(1)

with $\Delta\rho$ the contrast in neutron scattering length density between precipitates and matrix, V the volume of the cylinder ($V = \pi D^2 L/4$), and q_L and q_D the components of the scattering vector along the axis of the precipitate and in the cross-sectional plane of the precipitate, respectively. J_1 is the first-order Bessel function of the first kind. Since the intensity is expressed as the product of two functions, each depending on a single component q_L or q_D of the scattering vector, it is

apparent that the intensity behaves very differently along q_L and q_D, which gives rise to an anisotropic signal. The microstructure is composed of three orthogonal variants of β'' needles. We assume that each variant contributes one-third of the total precipitate volume fraction and that they all share the same (average) size. Since the sample has been cut with a [001] direction normal to its surface, one of the precipitate variants has its q_L component equal to zero on the detector. Its two-dimensional signal is then isotropic and depends only on D and not on L. The other two variants give rise to characteristic streaking (Fratzl *et al.*, 1993; De Geuser *et al.*, 2012), the long dimension of which is controlled by the Bessel function part of equation (1) (*i.e.* the diameter of the needles) and the thickness of which is controlled by the sine part of equation (1) (*i.e.* the length of the needles). The contrast ρ depends on the composition model for β''. We will test different composition assumptions from the literature (see §4.3). Within these assumptions, there are only three free parameters in the model, namely the dimensions of the precipitates, L and D, and their number density N (or their volume fraction $v = NV$, with $V = \pi D^2 L/4$).

A simultaneous fitting to the full two-dimensional distribution of scattering events acquired at the two detector distances was carried out. A nonlinear least-square fitting was performed by minimizing the following quantity:
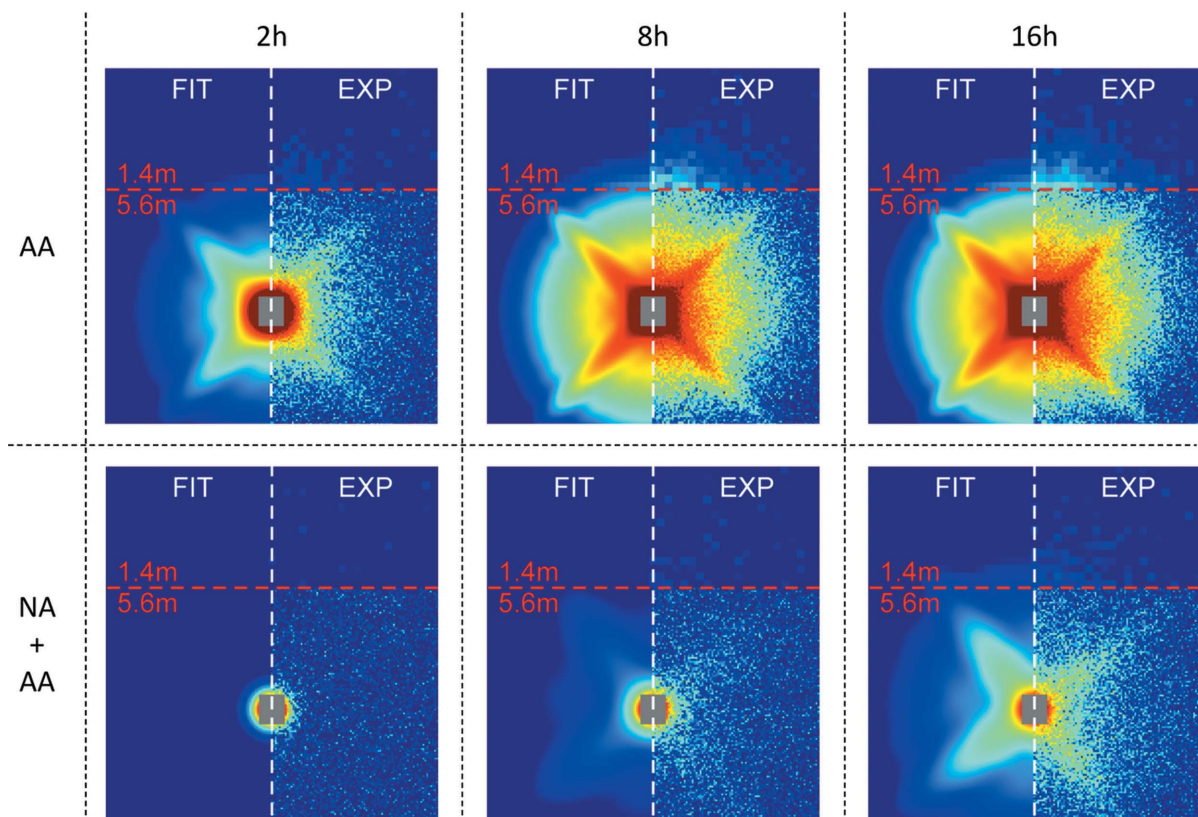
Figure 1
Experimental and fitted two-dimensional SANS patterns $I(\mathbf{r})$ for three ageing times (2, 8 and 16 h). The colour map for intensity I is the same for all the images. Top: AA sample. Bottom: NA + AA sample. The entire image sequence is shown as a video in the online supporting information (available from the IUCr electronic archives; Reference KS5456). (The first 30 images of each sequence are short 1 min acquisitions, while the subsequent sets were acquired every ~12 min.)

Cynthia Sin Ting Chang *et al.* · *In situ* characterization of β'' precipitation

research papers

$$\chi^2 = \sum_{\text{1st distance}} \left(\frac{I - I_{\text{fit}}}{\Delta I} \right)^2 + \sum_{\text{2nd distance}} \left(\frac{I - I_{\text{fit}}}{\Delta I} \right)^2, \quad (2)$$

where I and ΔI are the experimental intensities and experimental uncertainties at a given detector pixel. I_{fit} is the modelled intensity. To account for the Laue scattering of the

(a)

(b)

Figure 2
Radial scattering intensities calculated from two-dimensional SANS patterns by averaging over certain directions. The q range shown corresponds to the broken horizontal line in Fig. 1. (*a*) Data for AA and NA + AA and two AA times averaged over all directions. (*b*) Data for 16 h of AA averaged over restricted angles, namely over four 22.5°-wide sectors centred on the four streaks visible in Fig. 1 ('along streaks') and four sectors of the same width exactly in the middle between the streaks ('between streaks'). Points represent averages obtained from experimental two-dimensional data, while lines are derived from fitted two-dimensional data (note: these are not one-dimensional fits).
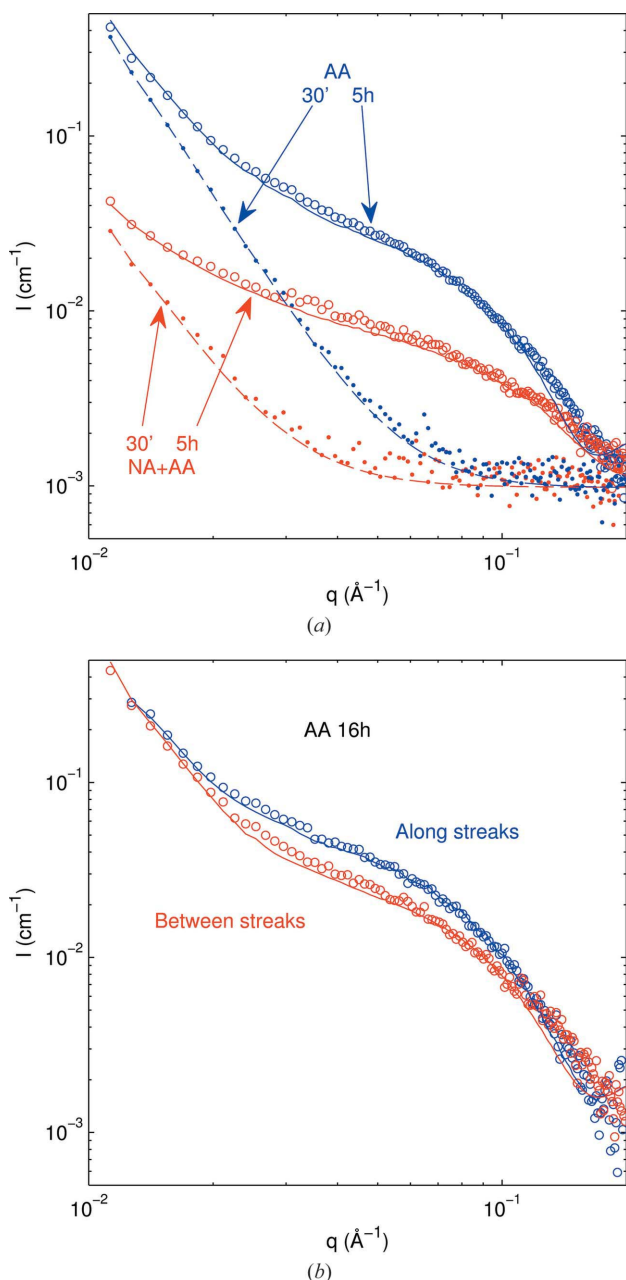
matrix as well as the incoherent scattering of the sample, a constant contribution is assumed. Existing large features (coarse precipitates, dislocations, grain boundaries, scratches, microvoids *etc.*) are considered to give rise to a Porod-type contribution. These two contributions lead to a background of the type $a + bq^{-n}$, which can be well fitted to the early images where no precipitation is detected. We find an exponent of 3.81 for AA and 3.5 for the NA + AA sample. As one expects $n = 4$ for volume scatterers with sharp interfaces, but smaller values for more diffuse boundaries or dislocations (Heuser, 1994), these values are consistent with a mixture of different contributions and justify the ansatz for the background correction. The incoherent background was found to be such that no significant difference could be measured between the initial sample's signals, although it is expected that the naturally aged sample contained a significant number of clusters. It can thus be concluded that the signal due to clustering is not sufficiently intense to be separated from the incoherent background. This is in line with a previous observation that two months of NA in an alloy with an even higher Mg and Si content than in the present alloy gave rise to only marginal extra scattering (Banhart *et al.*, 2010).

The fitting strategy was to start from the last annealing point and use the results of the nth point as starting value for the $(n - 1)$th point. This ensures fast convergence and good continuity of data. We considered the extracted values significant only when the χ^2 of the fit was lower than that obtained when only the contribution of the $a + bq^{-n}$ background was considered. This was typically not the case at the very beginning of precipitation when the volume fraction is too small to yield a significant SANS intensity.

3. Results

Fig. 1 shows two-dimensional scattering patterns for three ageing times for both experiments along with the fitted patterns. The patterns exhibit the typical fourfold symmetry generated by the collection of mutually perpendicular needle-shaped objects in the plane perpendicular to the incoming beam.

In order to be able to assess the absolute values of the colour-coded data of Fig. 1, averaged radial scattering intensities have been calculated (see Fig. 2). Averaging over all angles yields a single radial function, as shown in Fig. 2(*a*) for two ageing times and two heat treatments. Averaging only over the four streaks of the patterns in Fig. 1 gives us the graphs shown in Fig. 2(*b*) for one ageing time and heat treatment. Averaging over the direction between these four streaks yields another function. The procedure is carried out both for the experimental two-dimensional data sets and for the fitted two-dimensional patterns. Fig. 2 allows for an assessment of the quality of the two-dimensional fit as well as for more quantitative comparisons of different curves, which is difficult for the colour-coded data in Fig. 1. One observation is that the scattering intensity is always larger for the sample aged for 5 h compared to the one aged for 30 min, even at the highest q value in Fig. 2, which marks the beginning of the

values obtained at the shortest detector distance. We see that the contribution of the detector positioned at the short distance (high q values) is rather small but not negligible. In future one could consider sacrificing the high-q data by measuring only at the long detector distance, in order to increase the repetition frequency of the measurements without deteriorating the information obtained too much.

Fig. 3 shows the calculated length and diameter of β'' precipitates as well as their number density as a function of

AA time (left colum, a, c, e). The volume fraction and the aspect ratio of the precipitates have been calculated from these three values (right column, b, d, f). In a first step, the analysis is based on a composition Mg_5Si_6 for the precipitates.

For the AA sample, precipitates are detectable after ~1 h of AA. The analysis reveals a concomitant growth of both the length and the diameter (thickness) of precipitates. Within the first ~6 h, the length grows faster than the diameter, so that the L/D ratio increases from 4 to 8. After 6 h, the length
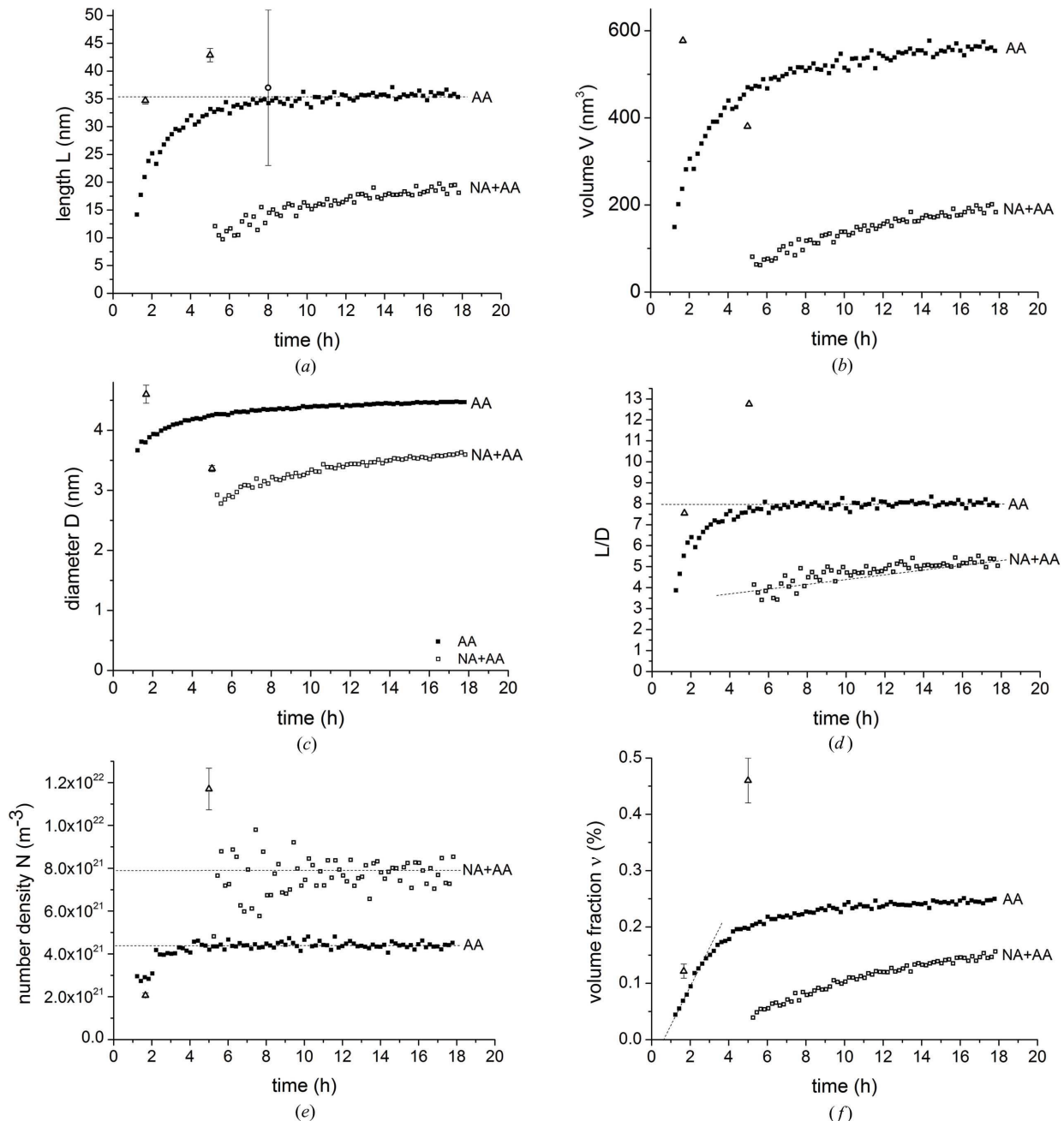
Figure 3
Parameters describing growth of precipitates in the Al–Mg–Si single crystal during *in situ* ageing at 453 K without (AA) and with one week of NA prior to AA (NA + AA). The analysis is based on a precipitate composition Mg_5Si_6. Data for NA + AA have been omitted for $t_{AA} < 5$ h owing to insufficient scattering. The left column (a), (c), (e) contains independent information (length L, diameter D, number density N), the right column (b), (d), (f) dependent data derived from the other three sets (precipitate volume $V = \pi D^2 L/4$, aspect ratio L/D and volume fraction $v = NV$). Dashed lines denote trends pointed out in §3. The circle corresponds to a value derived from Fig. 4; triangles denote experimental data for an alloy 6060 exposed to 30 min of NA before AA (Teichmann *et al.*, 2013). The times given refer to the beginning of the acquisition period for each data set, which lasts ~12 min.

remains almost constant and just the thickness increases very slightly (L/D decreases slightly). The volume fraction increases rapidly and almost linearly at the beginning and starts levelling off after 2.5 h. After 6 h, it increases only slowly. Extrapolation to zero volume fraction gives a time of $\sim\frac{1}{2}$ h, at which precipitation starts. The number density increases slightly for the period between 1 and 2 h, after which it reaches a plateau, the value of which is about 4.5×10^{21} m^{-3} assuming a composition Mg$_5$Si$_6$ for the precipitate (see also §4.3).

For the NA + AA sample, totally different kinetics of precipitate growth are observed. The length and thickness are much lower and also grow slower. A pronounced incubation time of $\sim$5 h is needed before precipitation can be detected by our setup. Both length and diameter increase slowly between 5 and 18 h, length at a slightly higher rate, which is why L/D increases from 3.5 to 5. The volume fraction of precipitates is also much lower than for the AA sample and grows gradually. The number density reaches a plateau value of 8×10^{21} m^{-3} (assuming Mg$_5$Si$_6$) within the first 5 h (when no data could be acquired) and remains constant for the rest of the experiment at a level which is about twice as high as for sample AA.

In the later stages of AA, for example after 10 h, longer and thicker β'' precipitates with a higher aspect ratio but a lower number density have formed during the AA experiment compared to the NA + AA experiment, but owing to the larger precipitate dimensions their volume fraction is higher.

4. Discussion

4.1. Precipitation kinetics

The nucleation stage, as defined by an increase in the precipitate number density, seems to be hardly detectable. Only in the first two hours of precipitation in sample AA can we suspect an increase in precipitate number density. After 2 h, no more apparent nucleation is observed and the number density remains constant. Therefore, this stage is characterized by pure growth of a constant number of precipitates, whereby their aspect ratio increases as they grow faster along their long axis than in thickness. This change in aspect ratio might be related to a gradual change in composition and/or structure of the precipitates, which can influence our measure of the volume fraction (*cf.* §4.3).

When ageing takes place directly after quenching, the solute and vacancy supersaturation are both at their highest possible level. This is why nucleation and growth progress fast and high volumes of precipitates are formed. In contrast, if the sample is naturally aged after quenching, a high density of atom clusters are formed, the precise structure of which is unknown but that are believed to contain a few tens of solute atoms per cluster only (Serizawa *et al.*, 2008). This leads to a decrease of solute supersaturation in the matrix and vacancies are either permanently lost, *e.g.* to grain boundaries, or temporarily trapped inside clusters. Subsequent AA therefore leads to a slower initial growth of precipitates. At AA temperature, small clusters tend to dissolve and release solute atoms to the matrix (Pashley *et al.*, 1967), which leads to the well known

decrease of hardness in the early stages of ageing [for about 1 h at 453 K for alloy AlMg0.4Si0.4 (Yan, 2014)] and a dissolution signal in the differential scanning calorimetry trace [above 453 K at a heating rate of 10 K min^{-1} for alloy AlMg0.4Si0.4 (Schmidt, 2010)]. This dissolution releases solute, increasing the supersaturation, eventually allowing precipitation to occur and larger clusters to evolve into precipitates detectable by SANS (Chang *et al.*, 2009). This situation gives rise to the increased number density shown in Fig. 3.

Finally, a comment on reproducibility. Owing to beam time restrictions the experiments could not be duplicated. Hardening experiments on corresponding polycrystalline samples, however, show that such hardening curves are well reproducible. This indicates that no erratic effects of the quenching procedure, storage at room temperature or re-heating are to be expected.

4.2. Comparison with TEM data

Fig. 4 shows a bright-field TEM image of the single crystal aged for 8 h at 453 K directly after quenching. The distribution of the longer axis of the precipitates in the image plane (two orientations) and perpendicular to this plane (one orientation) can clearly be seen. The observed length of the precipitates is predominantly <50 nm and the average length was calculated to be 37 (14) nm based on 44 precipitates, which corresponds well to Fig. 3. Such a low number of precipitates with such a wide size distribution, however, offers us no precise average value and the good agreement should be rather considered a conincidence. Owing to the concentration gradients found in
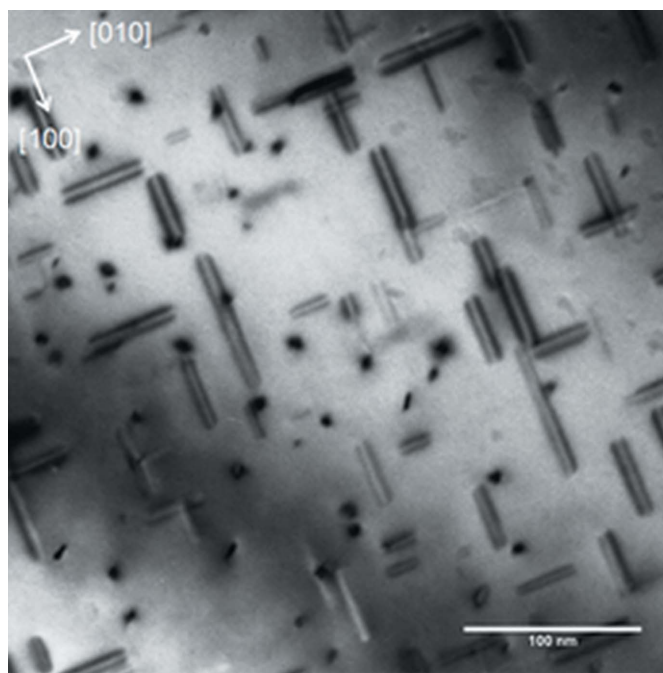
Figure 4
Bright-field TEM image of the single crystal aged at 453 K for 8 h directly after quenching (Chang *et al.*, 2012).

Table 1
Summary of the change of four parameters describing β'' precipitates in fully aged samples if one goes from direct ageing (AA) to ageing after an NA step before AA (NA + AA).

Trends are derived either from the literature as discussed in §4.2 or from Fig. 3. In the former case, an arrow shows the direction of the change as stated by the majority of the references, and a question mark points out inconsistencies in the literature.

Alloy	Length	Diameter	Volume fraction	Number density
Low in Mg and Si	↓	↓	↓?	↑
Low in Mg or Si	↓	↓	↓	↑?
This study	↓	↓	↓	↑
High in Mg and Si	↑	↑?	?	↓

the single crystal (see §2.1), a more extended quantitative comparison was not deemed meaningful, which is why no further TEM images are shown.

In the literature, a number of statistical analyses of β'' precipitate dimensions and number densities by transmission electron microscopy have been reported. Since the alloy compositions and heat treatments vary very much, the corresponding data also do so. Experimental TEM data for an alloy 6060 with an Mg and Si content close to that of the alloy used here (see compositional analysis reported in §2.1) are included in Fig. 3 for comparison with the SANS results. This alloy had been naturally aged for 30 min prior to AA and should thus be considered an intermediate state between AA and NA + AA. While the correspondence is not perfect, the precipitates' absolute dimensions and the trend for number density are in a fair agreement between the SANS and TEM results.

To further position our present results in the scope of the existing literature for these alloys, we shall now discuss the difference between AA and NA + AA and compare our values obtained by SANS with TEM data extracted from the literature. Some work is available in which artificial ageing experiments with and without prior NA are described. Comparing various sources we find that some sources state that β'' precipitates become longer and thicker (or have the same thickness) after a given AA time if the alloy is subject to NA before AA. This applies to alloys 6111 (Wang et al., 2003), 6061 (Pogatscher et al., 2013), 6082 (Marioara et al., 2003; Cuniberti et al., 2010), AlMg0.6Si0.8 (Liang, 2009) and AlMg0.8Si0.9 (Torsaeter, 2011). Other sources report shorter and thinner β'' precipitates after a given AA time if the sample is subject to NA before AA. This is found for alloys AlMg0.4Si0.4 (Liang, 2009; Torsaeter, 2011), AlMg0.4Si0.8 and AlMg0.9Si0.4 (Wenner et al., 2012). This suggests a trend that, whenever the content of both Mg and Si is 'high' (i.e. ≥ 0.6%), NA before AA leads to longer and thicker precipitates, whereas if the content of one or both of the alloying elements is 'low', the opposite is true. This finding has been documented as a kind of 'majority vote' (see second and third columns in Table 1).

In this respect, our measurements of the evolution of thickness and length correspond to the behaviour found for alloys with a low content of Mg or Si, which is in agreement

with the measured average composition of 0.43%Mg and 0.47%Si of our alloy. However, one should not go too far with such comparisons, because especially the thickness of β'' precipitates is not easy to measure and the statistics of TEM data are usually poor. Moreover, the absolute values for the precipitate dimensions differ a lot in the literature because of the varying alloy compositions and heat treatment procedures.

The number density of β'' precipitates formed during AA has also been measured by TEM. Alloys high in Si and Mg have been found to show a lower number density in the aged condition if NA has taken place before for alloy 6111 (Wang et al., 2003), alloy 6082 (Cuniberti et al., 2010; Marioara et al., 2003), alloy AlMg0.6Si0.8 (Liang, 2009), alloy 6061 (Pogatscher et al., 2013) and alloy AlMg0.8Si0.9 (Torsaeter, 2011). Alloys low in Mg or Si show a slightly higher or the same number density for AlMg0.4Si0.4 (Liang, 2009; Torsaeter, 2011), as well as for AlMg0.4Si0.8 (Wenner et al., 2012) and AlMg0.9Si0.4 (Wenner et al., 2012). Our SANS data indicate that the number density of precipitates after AA is higher if NA has been performed prior to AA. In this respect, our alloy again represents a situation closer to the alloys low in Mg or Si.

The total volume fraction of β'' precipitates formed during AA is calculated from the dimensions of the precipitate and their number density. Here, the data in the literature are less consistent than for the other parameters. The alloys high in Si and Mg have been found to show a lower volume fraction of precipitates in the aged condition if NA has taken place before for alloy 6111 (Wang et al., 2003) and alloy 6082 (Cuniberti et al., 2010; Marioara et al., 2003), but alloys AlMg0.6Si0.8 (Liang, 2009) and AlMg0.8Si0.9 (Torsaeter, 2011) show the opposite trend. Alloys low in Mg or Si show a decrease for AlMg0.4Si0.4 (Liang, 2009; Torsaeter, 2011), AlMg0.4Si0.9 and AlMg0.9Si0.4 (Wenner et al., 2012). Our SANS results indicate that the volume fraction is always lower for NA + AA than for direct AA, which is in line with most of the data from the literature.

Some authors have distinguished between various populations of precipitates in later stages because they find a few large high-volume precipitates (Pogatscher et al., 2013; Wang et al., 2003). Our SANS analysis provides an effective value for the length and diameter only, and we might be averaging over such bimodal distributions. Still, we conclude that the sample we investigated by SANS shows a difference between AA and NA + AA which is typical for alloys with a low Mg or Si content but is different from alloys high in both Mg and Si.

4.3. Influence of precipitate composition

We have to assume a composition for the precipitates and have taken Mg_5Si_6, which is one of the accepted stoichiometries of the β'' phase (Zandbergen et al., 1997. This assumption will have an impact on the number density (and volume fraction) of precipitates but not on their length and diameter. There is, however, a dispute about the exact composition of β'' precipitates in the peak aged condition. It is now generally accepted that Al atoms in addition to the solute Mg and Si

atoms are contained in the β'' precipitates, at least at some stage of growth. It is also known that the composition of precipitates changes during their evolution because of the repulsion of Al and inclusion of solute atoms, not only in 6xxx alloys (Chen *et al.*, 2006; Marceau *et al.*, 2013) but also in other alloys, *e.g.* 7xxx alloys (De Jong *et al.*, 2012).

We illustrate this by displaying the volume fraction and number density of precipitates as calculated from the SANS data while using both Mg_5Si_6 and the composition $Mg_5Si_4Al_2$ derived from atom probe and electron diffraction observations and *ab initio* calculations (Hasting *et al.*, 2009). Fig. 5 (open symbols) shows the result of this analysis. According to these results, both the volume fraction and number density are about 20% higher when they are based on $Mg_5Si_4Al_2$ rather than on Mg_5Si_6. The reason for this is that Al in the precipitate hardly contributes to the scattering length difference from the surrounding matrix and a higher volume fraction of precipitates is needed to represent the measured scattering if Al is contained in the precipitate. Mg has a higher absolute scattering length than Si and both are higher than that of Al. An increased Mg or Si content would therefore decrease the

volume fraction and number density, for Mg more than Si. This is even better seen from the full symbols in Fig. 5, which correspond to structures containing even more Al and different amounts of Mg and Si and have been postulated to be pre-stages of the final β'' precipitates. Such compositions are only valid in very early stages of precipitation. In later stages, compositions reflected by the open symbols in Fig. 5 are more realistic. In any case, these facts should be kept in mind when considering the volume fractions and number densities in Fig. 3. Since we assumed a composition Mg_5Si_6 for the plots in Fig. 3, the absolute values should be interpreted as a minimum. Provided that the precipitates have the same (or similar) compositions for both samples, a relative comparison is always valid.

5. Conclusions

Small-angle neutron scattering (SANS) has been successfully used to monitor the growth of β'' precipitates in an Al–Mg–Si alloy *in situ* during artificial ageing. Use of an oriented single crystal allowed us to determine both the length and the thickness (= diameter) of the precipitates independently, along with their number density, by assuming that a collection of 'average' precipitates of equal size was formed. The time resolution of the measurement was about 12 min, thus allowing for a much more detailed study of precipitation kinetics than, for example, by TEM.

β'' precipitates were found to grow in volume throughout the observable range of precipitation. They grow more in length than in thickness. Direct artificial ageing after quenching produces fewer but larger precipitates of a higher total volume than artificial ageing after natural pre-ageing.

The values obtained for length, thickness and number density qualitatively coincide with data derived from TEM images of different alloys. The impact of NA before AA on length, thickness and number density of precipitates after a fixed AA time is also in coincidence with most of the TEM-related data found in the literature for alloys that contain less than 0.6% of either Mg or Si.

While SANS was shown to provide information compatible with TEM, it provides data averaged over much larger volumes (containing $\geq 10^{15}$ precipitates), allows for *in situ* measurements on one sample and provides a time resolution that is hard to obtain by TEM in practice (69 or 85 data points in one ageing cycle).

Future work would benefit from samples with a more uniform concentration, which we could not obtain. This would allow one to measure the hardness curve and other data and to obtain samples for TEM and atom probe measurements. TEM images taken at selected ageing times could then be used to check whether there are any anomalies in the size distribution that could affect the SANS analysis. Atom probe measurements could provide the actual (possibly time-dependent) concentration of the precipitates, which could be used to calculate a time-dependent scattering length density and to correct the volume fractions now calculated assuming a constant composition.
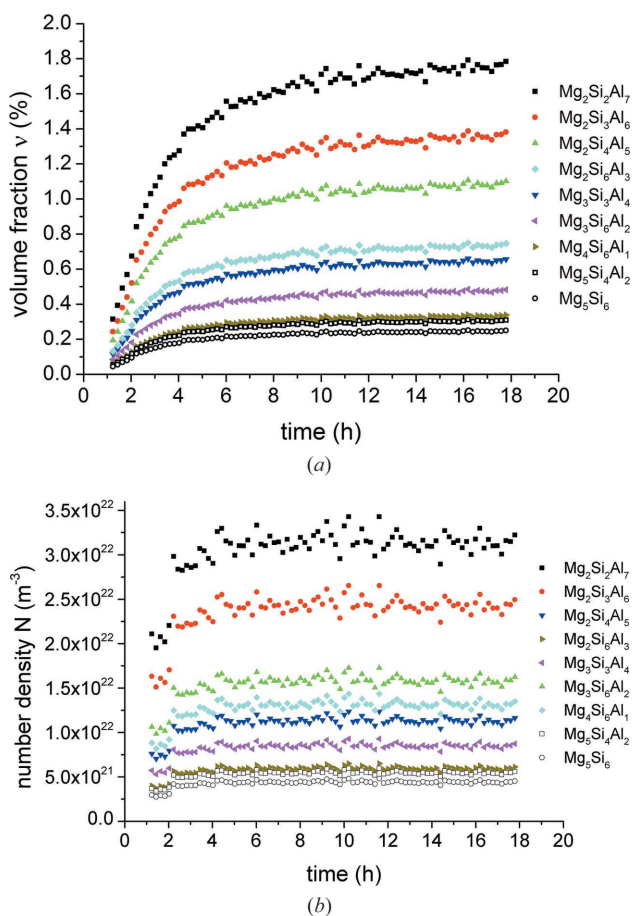
Figure 5
Precipitate volume fraction (*a*) and number density (*b*) for experiment AA calculated from SANS data using different precipitate compositions. Filled symbols: compositions of pre-stages of β'' precipitates supposed to be occurring sequentially during ageing (Chen *et al.*, 2006). Open symbols: compositions suggested for fully evolved β'' precipitates (Hasting *et al.*, 2009; Zandbergen *et al.*, 1997)

References

Abis, S., Boeuf, A., Caciuffo, R., Fiorini, P., Magnani, M., Melone, S., Rustichelli, F. & Stefanon, M. (1985). *J. Nucl. Mater.* **135**, 181–189.

Abis, S., Caciuffo, R., Coppola, R., Fiorini, P., Rustichelli, F., Magnani, M. & Stefanon, M. (1987). *Mater. Sci. Forum*, **13–14**, 295–300.

Albertini, G., Caglioti, G., Fiori, F. & Pastorelli, R. (2000). *Phys. B Condens. Matter*, **276–278**, 921–922.

Banhart, J., Chang, C. S. T., Liang, Z. Q., Wanderka, N., Lay, M. D. H. & Hill, A. J. (2010). *Adv. Eng. Mater.* **12**, 559–571.

Banhart, J., Lay, M. D. H., Chang, C. S. T. & Hill, A. J. (2011). *Phys. Rev. B*, **83**, 014101.

Bardel, D., Perez, M., Nelias, D., Deschamps, A., Hutchinson, C. R., Maisonnette, D., Chaise, T., Garnier, J. & Bourlier, F. (2014). *Acta Mater.* **62**, 129–140.

Brenner, P. & Kostron, H. (1939). *Z. Metallkd.* **31**, 89–97.

Chang, C. S. T., Heinemann, A., Dewhurst, C., Liang, Z. & Banhart, J. (2012). *13th International Conference on Aluminium Alloys (ICAA13)*, edited by H. Weiland, A. D. Rollett & W. A. Cassada, pp. 1083–1088. Pittsburgh: TMS and Wiley.

Chang, C. S. T., Wieler, I., Wanderka, N. & Banhart, J. (2009). *Ultramicroscopy*, **109**, 585–592.

Chen, J. H., Costan, E., van Huis, M. A., Xu, Q. & Zandbergen, H. W. (2006). *Science*, **312**, 416–419.

Cuniberti, A., Tolley, A., Riglos, M. V. C. & Giovachini, R. (2010). *Mater. Sci. Eng. A*, **527**, 5307–5311.

De Geuser, F., Bley, F. & Deschamps, A. (2012). *J. Appl. Cryst.* **45**, 1208–1218.

De Geuser, F. & Deschamps, A. (2012). *C. R. Phys.* **13**, 246–256.

Dewhurst, C. (2008). *GRAS$_{ans}$P*, http://www.ill.eu/lss/grasp/.

Donnadieu, P., Carsughi, F., Redjaimia, A., Diot, C. & Lapasset, G. (1998). *J. Appl. Cryst.* **31**, 212–222.

Fratzl, P., Langmayr, F. & Paris, O. (1993). *J. Appl. Cryst.* **26**, 820–826.

Gayler, M. L. V. & Preston, G. D. (1929). *J. Inst. Met. London*, **41**, 191–247.

Guinier, A. & Fournet, G. (1955). *Small-Angle Scattering of X-rays*. New York: Wiley.

Hasting, H. S., Froseth, A. G., Andersen, S. J., Vissers, R., Walmsley, J. C., Marioara, C. D., Danoix, F., Lefebvre, W. & Holmestad, R. (2009). *J. Appl. Phys.* **106**, 123527.

Heuser, B. J. (1994). *J. Appl. Cryst.* **27**, 1020–1029.

Jong, M. de, van der Zwaag, S. & Sluiter, M. H. F. (2012). *Int. J. Mater. Res.* **103**, 972–979.

Liang, Z. Q. (2009). Thesis, South China University of Technology, People's Republic of China.

Lyon, O., Davis, B. E. C., Hoyt, J. J., Pro, R., Simon, J. P., Warburton, W. K. & Defontaine, D. (1983). *JOM J. Min. Met. Mater. Soc.* **35**, 68.

Marceau, R. K. W., de Vaucorbeil, A., Sha, G., Ringer, S. P. & Poole, W. J. (2013). *Acta Mater.* **61**, 7285–7303.

Marioara, C. D., Andersen, S. J., Jansen, J. & Zandbergen, H. W. (2003). *Acta Mater.* **51**, 789–796.

Ohnuma, M. & Suzuki, J. I. (2006). *Bunseki Kagaku*, **55**, 381–390.

Pashley, D. W., Jacobs, M. H. & Vietz, J. T. (1967). *Philos. Mag.* **16**, 139.

Pashley, D. W., Rhodes, J. W. & Sendorek, A. (1966). *J. Inst. Met. London*, **94**, 41–49.

Pogatscher, S., Antrekowitsch, H., Leitner, H., Sologubenko, A. S. & Uggowitzer, P. J. (2013). *Scr. Mater.* **68**, 158–161.

Schiffmann, R., Haug, J. & Banhart, J. (2004). *9th International Conference on Aluminium Alloys (ICAA-9)*, edited by B. C. Muddle, A. J. Morton & J.-F. Nie, pp. 604–609. Melbourne Institute of Materials Engineering Australia.

Schmidt, E. (2010). Thesis, TU Berlin, Germany.

Serizawa, A., Hirosawa, S. & Sato, T. (2008). *Metall. Mater. Trans. A*, **39**, 245–251.

Teichmann, K., Marioara, C. D., Pedersen, K. O. & Marthinsen, K. (2013). *Mater. Sci. Eng. A*, **565**, 228–235.

Torsaeter, M. (2011). Thesis, Norwegian University of Science and Technology, Trondheim, Norway.

Tsao, C. S., Chen, C. Y., Jeng, U. S. & Kuo, T. Y. (2006). *Acta Mater.* **54**, 4621–4631.

Wang, X., Poole, W. J., Esmaeili, S., Lloyd, D. J. & Embury, J. D. (2003). *Metall. Mater. Trans. A*, **34**, 2913–2924.

Wenner, S., Marioara, C. D., Andersen, S. J. & Holmestad, R. (2012). *Int. J. Mater. Res.* **103**, 948–954.

Yan, Y. (2014). PhD thesis, Technische Universität Berlin, Germany.

Zandbergen, H. W., Andersen, S. J. & Jansen, J. (1997). *Science*, **277**, 1221–1225.